Determining Neutralino Mixing Properties

Colm Murphy, University College London, England

September 8, 2016

Abstract

Supersymmetry aims to explain the dark matter content of the universe. It provides the $\tilde{\chi}_1^0$ as the candidate particle. Is this the only contributor to dark matter? To quantify and verify this we need to be able to measure neutralino mixing. In thus study we aim to determine which experimental observables could be analysed to measure the neutralino mixing matrix.

Contents

1. Introduction

One of the main shortcomings of the standard model (SM) is that is lacks an explanation for dark matter. As experimental observations have shown that approximately 26.8% of the universe's mass is made up of dark matter, compared to only 4.9% of the ordinary matter explained by the standard model, coming up with an explanation for dark matter is a primary motivation of many models beyond the standard model [1]. The amount of dark matter present in the universe is quantified through the dark matter relic density, Ω. This has been measured by the ESA Planck mission to roughly 2% uncertainty. If a model beyond the standard model is to account for our observations of dark matter then it must predict and explain this number.

Dark matter could come from a particle, which is of particular interest because perhaps this particle could be detected at the ILC. However, the standard model does not predict any suitable dark matter candidate particle.

Supersymmetry is a model beyond the standard model which does have a dark matter candidate particle. This particle is governed by a mixing matrix. In a previous study, one of these mixing matrix elements was found to effect dark matter relic density fairly strongly [2]. If we could find a way of measuring this mixing element, then we could make predictions about the relic density and potentially find out if this supersymmetric particle accounts for all of the observed dark matter in the universe or not. This is the purpose of this study - to find direct experimental observables which could be used to measure this mixing matrix.

2. Theory

2.1. The ILC

The International Linear Collider (ILC) is a proposed future linear collider. It would collide electrons and positrons together with a centre of mass energy of 500 GeV, with the potential to be upgraded to 1000 GeV [3]. One of the important properties of the ILC which is mentioned in this report is its ability to tune the polarisations of each beam. The electron beam can be polarised up to 80% and the positron beam can be polarised up to 30% [4]. The notation used to describe the beam polarisation combinations is as follows:

$$\mathcal{P}(e^{-}polarisation, e^{+}polarisation)$$

For example, one of the combinations used in this study is $\mathcal{P}(-0.8, +0.3)$. The negative sign means left handed polarisation (LH), and the positive sign means right handed polarisation (RH). So this example combination means that the electron beam is 80% left handed polarised and 20% unpolarised, i.e. approximately 90% left handed and 10% right handed.

2.2. Software

Here I will briefly introduce the two most commonly used programs in this study, as they are often mentioned and were essential to the experimental procedure of this work.

2.2.1. SPheno

SPheno is one of the programs which was used heavily in this project. It is a spectrum calculator, which means that it takes a certain set of initial condition parameters for a given theory (in our case the MSSM), and uses the relevant renormalisation group equations (RGE) to calculate what masses particles would have at our energy scale after being run down from the grand unified energy scales of SUSY, as well as other parameters and observables [5]. It was used in this study to scan the parameter space, and analysis was performed on the masses, branching ratios and mixing elements produced by it.

2.2.2. Whizard

Whizard is an Monte Carlo event generator which was also used heavily in this study [6]. It was used to simulate ILC like collisions between electrons and positrons at a 500 GeV centre of mass energy. For each collision it calculated the cross sections, product particles, and also called further software (namely PYTHIA [7]) to compute the fragmentation of unstable daughter particles. The number of events to generate, the beam polarisation conditions to consider, the process channels to input and more can all be specified. These features were used in this study so that separate analysis could be performed depending on which ILC beam polarisation combination was being used, and which channel we were interested in analysing. Whizard can take SPheno output files as input steering files, so these two programs were used together in a complimentary manner throughout the study.

2.3. Supersymmetry

Supersymmetry is an extension of the standard model. It predicts the existence of superpartners for each current standard model particle, differing by half a unit of spin. As such bosons have superpartner fermions and fermions have superpartner bosons. The fermionic superpartners to standard model gauge fields are called gauginos. Additionally, standard model scalars (Higgs) has a fermionic partner Higgsino, and as well as this SUSY has an additional Higgs doublet and Higgsino. The scalar superpartners to the standard model fermions are the squarks and sleptons. The superpartner of a particle is generally indicated by the presence of a tilde, for example the $\tau \rightarrow \tilde{\tau}$, and is written by preceding the standard model name with an s: tau $\rightarrow$ stau.

Supersymmetry predicts that the only difference between the particles and their superpartners is the spin quantum number. However, superpartners have not yet been

detected, which means that supersymmetry must necessarily be broken, as the masses must be higher than the energies currently accessible at the LHC [8]. In this sense the standard model is an effective theory, which is UV completed by broken supersymmetry.

Supersymmetry is attractive for a number of reasons. It solves certain problems which arise in the standard model. For example, interactions between the Higgs and the standard model particles should mean that the Higgs would be very heavy, however this is not the case. Supersymmetric contributions to the Higgs mass would cancel out those added by the standard model particles, resulting in the light Higgs mass which has been observed [9].

Within supersymmetry, the three standard model forces of electromagnetism, weak and strong nuclear would unify at high energies. This grand unified theory is a strong motivation for many physicists who believe that the universe must have some kind of underlying beauty and overarching symmetry [10].

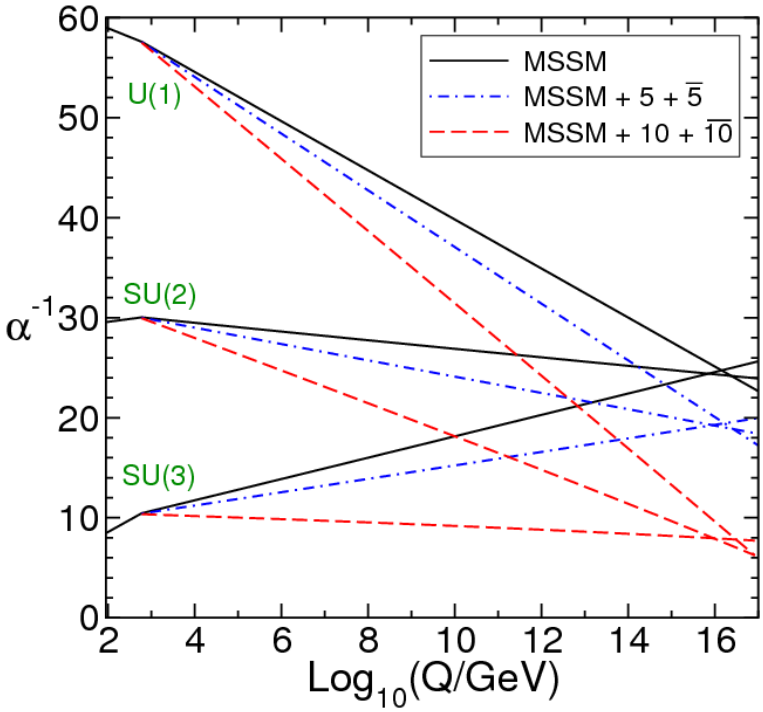

Figure 1: Plot showing unification of gauge couplings in SUSY.

Evidence for supersymmetry could be detected at the ILC via the direct production of superpartners. The annihilation of electron positron pairs with sufficient energy could result in the production of SUSY particles, for example neutralinos and charginos. However, there are many free parameters in SUSY, and different variations and scenarios predict different particle masses - so whether or not anything will be detected at ILC depends on the masses of the superpartners and whether or not they lay in the accessible range of energies. However there is reason to believe that if there is SUSY, at least some

particles will be within the ILC's initial range of $\sqrt{s} = 500$ GeV [11]. If not, then we know that the gauge bosons of the standard model are in this range, and thus precision studies not possible at the LHC can be carried out on them at the ILC.

Whilst these factors are all strong motivations for supersymmetry in general, the primary focus of this study needs only one thing: the provision of a supersymmetric dark matter candidate particle.

Supersymmetry naturally produces a dark matter candidate particle. This is the lightest supersymmetric particle (LSP), the neutralino one ($\tilde{\chi}_1^0$). It is a suitable candidate because it is stable, electrically neutral and interacts weakly with the standard model particles. It is stable because the MSSM conserves R parity multiplicatively. Each superparticle is assigned an R parity unit of -1, and each particle a unit of +1. R parity must be conserved at every vertex, so each superparticle must decay into one other, meaning the lightest particle must be stable as there is no available SUSY particle for it to decay into.

As briefly mentioned previously, the dark matter candidate of supersymmetry, the LSP (along with all other neutralinos), has its mass governed by the neutralino mass mixing matrix [12]:

$$\begin{pmatrix} M_1 & 0 & -m_Z c_\beta s_W & m_Z s_\beta s_W \\ 0 & M_2 & m_Z c_\beta c_W & -m_Z s_\beta c_W \\ -m_Z c_\beta s_W & m_Z c_\beta c_W & 0 & -\mu \\ m_Z s_\beta s_W & -m_Z s_\beta c_W & -\mu & 0 \end{pmatrix}$$

Here $s_W \equiv \sin\theta_W$, $c_W \equiv \cos\theta_W$, $s_\beta \equiv \sin\beta$ and $c_\beta \equiv \cos\beta$.

Note that here we can see the presence of the MSSM parameters M_1 and M_2. In my experimental procedure these parameters are varied in order to change the neutralino mixing matrix. Their presence in this matrix is why altering them results in different neutralino mixing matrix values.

This mass matrix is diagonalised by the matrix N_{ij}, where each component shows the relative contribution of the SUSY force particle to a given neutralino. For example, the N_{11} element, which is of particular importance in this study, decides the 'Bino-ness' of the LSP. The full expansion for the LSP is:

$$\tilde{\chi}_1^0 = N_{11}\tilde{B} + N_{12}\tilde{W}^3 + N_{13}\tilde{H}_d^0 + N_{14}\tilde{H}_u^0$$

Where this is simply the first line of the matrix equation which determines mass for all four of the neutralinos:

$$\tilde{\chi}_i^0 = N_{ij} \begin{pmatrix} \tilde{B} \\ \tilde{W}^3 \\ \tilde{H}_d^0 \\ \tilde{H}_u^0 \end{pmatrix}$$

Where these elements satisfy a unitarity condition (e.g. for the LSP):

$$1 = N_{11}^2 + N_{12}^2 + N_{13}^2 + N_{14}^2$$

2.4. Dark matter relic density, Ω

Dark matter relic density (Ω) is a measure of how much dark matter is currently present in the universe. If supersymmetry is to fully explain dark matter then it must be able to accurately predict this relic density. This need not mean that all of the observed dark matter is explained by the LSP, but it should be able to explain it at least in part. If the LSP contribution is lower than the observed amount, then there could be other contributing processes to the relic density. If it is too high then some other processes could cancel out this contribution to make it in line with experimental observation, however most believe the observed value to be an upper bound on theoretical predictions. Dark matter relic density has been measured accurately by the ESA Planck mission. In 2015 it measured the relic density to be $\Omega = 0.1197 \pm 0.0022$, an uncertainty of around 2% [1].

Many scenarios within supersymmetry predict a superpartner particle which is very close in mass to the LSP. This study looks at such a 'coannihilation scenario', where the LSP is almost degenerate in mass with the stau ($\tilde{\tau}^{\pm}$). It is so called because in this kind of scenario the LSP can coannihilate with the partner which is close to it in mass. This type of scenario is of particular interest because it tends to predict a dark matter relic density which is very close to the experimentally measured value. The properties and constraints on the dark matter candidate particle and its coannihilation partner are fairly strict, so the fact that the MSSM predicts the same result for relic density as the experimentally measured value is significant and warrants further investigation [13]. It seems to indicate that perhaps there is something important about models where this coannihilation is present, as there is no fundamental reason as to why the predicted relic density (calculated from SUSY models using the software micrOMEGAs [14]) should be anywhere even close to the experimental value. The specific set of MSSM parameters looked at in this study is called the STC8 point, and has been the subject of previous studies [2]. During the process of this study however, two of the parameters, namely M_1 and M_2, were varied from their original STC8 values.

Previous studies have found that small variations in the N_{11} element of the neutralino mixing matrix corresponds to a proportionally large variation in dark matter relic density [2]. Thus by accurately measuring the neutralino mixing at the ILC, relic density could potentially be determined. Further to this objective, an observable which corresponds to the neutralino mixing, which could be measured at the ILC, is needed. By measuring this observable the neutralino mixing and hence the dark matter relic density could be determined.

3. Measurement

3.1. Method

The purpose of this study was to find viable options for the experimental determination of the N_{11} neutralino mixing matrix element. In order to be able to measure this directly, we need to see which experimental observables vary when the value of N_{11} changes. So the first step was to identify points in the parameter space which generated differing N_{11} values.

To this end I wrote a script which ran SPheno for different combinations of M_1 and M_2. I looped between $M_i = 150 \rightarrow 300$ GeV for $i = 1$ and 2.

This script wrote out the relevant quantities from each SPheno output file to a plain text file, which could then be read in by Matlab. Please see Appendix A for the full list of relevant results generated by SPheno for each point. By plotting the neutralino mixing matrix elements versus M_1 and M_2 I could see at which points in the parameter space the change in N_{11} was most dramatic - see Figure 2. By doing this I decided that the best option was a diagonal path along a monotonic but non-linearly decreasing section in N_{11}. There were five points, with M_1 ranging from $210 \rightarrow 250$ GeV whilst M_2 ranged downwards from $250 \rightarrow 210$ GeV, both in steps of 10. For clarity I have included these points in Table 3.1, along with the naming convention used.

Point	M_1 / GeV	M_2 / GeV
A	210	250
B	220	240
C	230	230
D	240	220
E	250	210

Table 1: M_1 and M_2 values at each point

It is worth noting that generating different N_{11} points in the parameter space is not as simple as simply varying the value of N_{11} itself. Because this element comes from the neutralino mixing matrix as a whole, and this must satisfy certain unitarity conditions, changing one value without accounting for the others would be physically incorrect and would produce invalid results. By instead changing M_1 and M_2 and rerunning SPheno, I knew that I had generated a reliable and accurate mixing matrix, upon which further analysis could be carried out.

Once these five points had been identified, I ran SPheno once again for each point. This produced five output files which could be used as steering files for the Whizard event generator. The event generator was used to simulate e^+e^- collisions such as those at the ILC, for $\sqrt{s} = 500$ GeV. This generated data which could be analysed further using ROOT. For each run of the event generator, I specified the number of events to be 100 000, and gave each process as a separate run of the program. Furthermore,

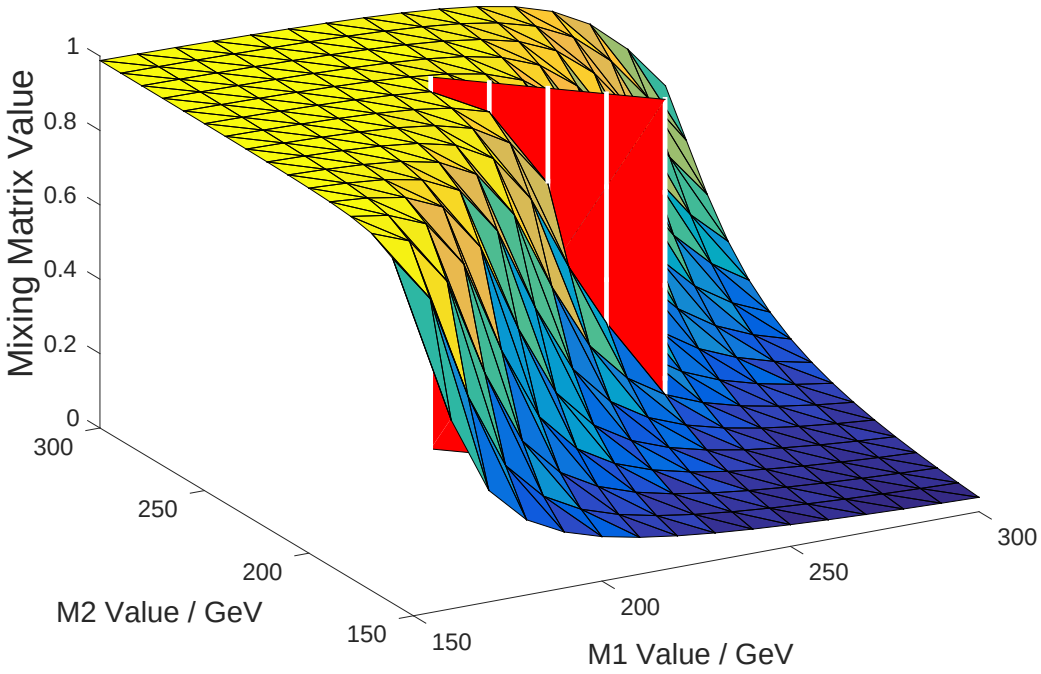

Figure 2: Plot showing N_{11} variation with M_1 and M_2. This plot was used to identify the five points to be investigated further. The red plane shows the path along the parameter space which was chosen. The white vertical lines represent the five equally spaced points.

both polarisation combinations of the colliding beams were ran separately. This way I could get different output files for each process and polarisation, allowing me to perform separate analysis on each. This differentiation was important, because some channels were more promising than others for providing ways to measure N_{11}, so isolating and analysing them separately was desirable. Once Whizard had ran for all of these separate processes, the files were converted from the standard stdhep format into slcio, and from that into lctuples for analysis with ROOT. All in all 40 files were to be analysed using ROOT. (5 N_{11} points $\times$4 process channels $\times$2 beam polarisation combinations).

3.2. Cross sections

One of the first avenues to be investigated was the cross section. For this the data generated by SPheno was used. Each run of SPheno produces an output file with information on branching ratios, particle masses and mixings, and cross sections. By setting up a simple script to read out cross section data from each N_{11} point in turn,

plots could be generated. I plotted each process's cross section separately. For each point polarisation was also varied, i.e. SPheno output two sets of cross sections for each file, one for each polarisation combination. These were plot as two lines on the same graph. By varying polarisation we could potentially gain another way to experimentally verify the N_{11} value.

Also note that whilst results are presented in this study for only N_{11} for the sake of clarity and because of its importance in determining the relic density, a similar treatment was carried out for the other matrix elements. Please see Appendix B for an example graph showing results for the matrix elements N_{ij} for $i, j = 1, 2$.

The cross section for the process $e^+e^- \to \tilde{\chi}_1^0\tilde{\chi}_2^0$ versus N_{11} is shown below.

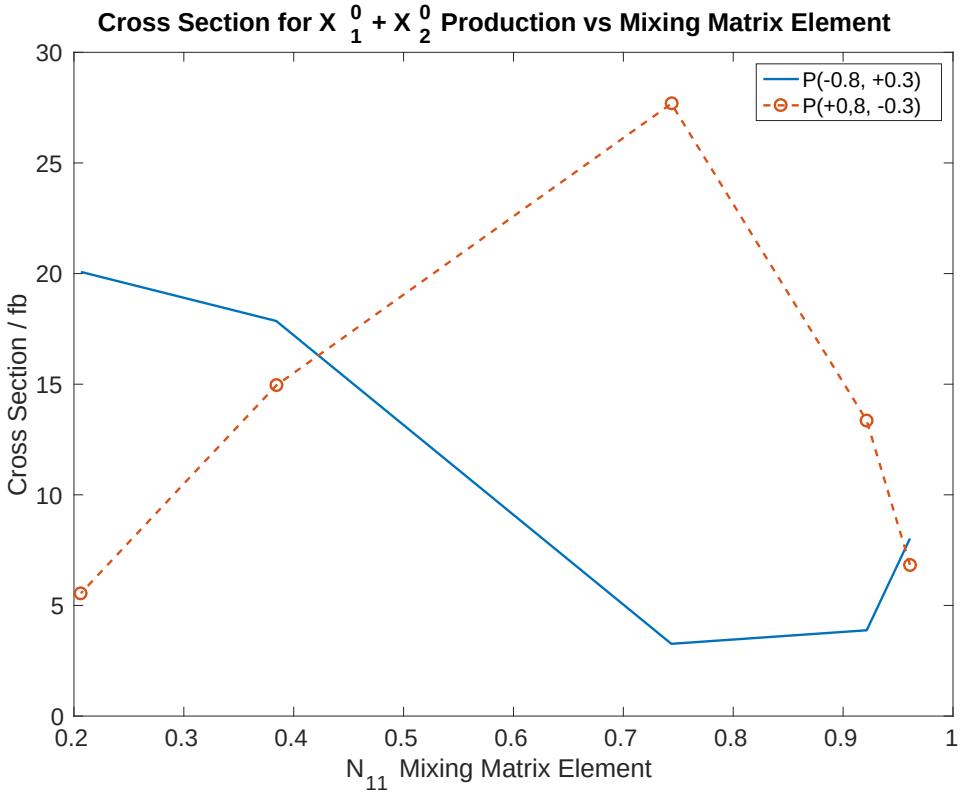

Figure 3: Plot showing cross section variation with N_{11}. Cross section appears to vary fairly strongly with N_{11} and differs fairly significantly depending on beam polarisation combination.

If the ILC discovers this MSSM scenario and the cross section of this process is measured to be roughly 20 fb for $\mathcal{P}(-0.8, +0.3)$, but changing to around 5 fb when beam polarisation is switched to $\mathcal{P}(+0.8, -0.3)$, then these experimental measurements would place N_{11} around 0.2. This production cross section seems to be a promising option for direct experimental measurement of N_{11}.

However, exploring cross sections in this way comes with an important caveat. When we see differences between the experimental observable in question (here cross section) at different N_{11} points, we want to ensure that this change is due almost entirely to changes in neutralino mixing. If this was not the case then it would be difficult to say that changes in experimental observables were due to changes in neutralino mixing, which would invalidate our results, as we are looking for ways to probe the neutralino mixing elements, and not other properties of the parameter space. In Figure 4 it can be seen that neutralino mass also varies from point to point. However this is to be expected because of the changes in the neutralino mixing matrix. This changes how much of each SUSY force particle contributes to the neutralino mass, so it is natural that the total mass value should vary. However, it can also be seen that the $\tilde{\tau}$ mass is essentially constant, so changes in slepton mass should not be a major factor interfering in the results of this study. It is important to note that the phase space reduces towards the middle point, and then wides out again from C $\rightarrow$ E. This has kinematic consequences which act to reduce the cross section at the middle point, because the matrix element is suppressed slightly due to the lower phase space. This must be accounted for when considering cross sections as a method for N_{11} measurement. Fortunately, as we have all of the mass and mixing data generated by SPheno for each point, then the changes in cross section due to reduced phase space calculable and can be taken into account. The dramatic changes in cross section seen in Figure 3 are too large to be due to simply these effects, so we can conclude that neutralino mixing must play the most important role.

Returning to Figure 4, we can see that the mass distribution is roughly symmetric about the point C. This would mean that if cross section (or any other experimental observable) were varying simply because of the mass differences involved, then the observable at point A and at point E should look roughly the same. Examining Figure 3 we see that the primarily right handed electron beam polarisation combination (dotted line) returns to a similar value from point A $\rightarrow$ E, however the same is not observed for the solid line polarisation. This means that not all of the effects here are accounted for by the phase space changes, and that neutralino mixing has a significant enough effect for this cross section measurement to be used as a method to probe the mixing matrix elements.

3.3. Branching ratios

Moving on from cross sections, decay branching ratios were also examined. By measuring how often produced particles (neutralinos or charginos) decay into certain daughter particles, one could gain information on the mixing matrix. Of course any fragment particle produced in the large chain of decays after the initial e^+e^- annihilation can be analysed, but we are mainly interested in those involving neutralinos and charginos, which would naturally give the most information on mixing. This branching ratio analysis does not include the $\tilde{\chi}_1^0\tilde{\chi}_1^0\gamma$ channel, because other than emitting final state radiation (i.e. more γs) no fragment particles are produced, due to the stability of the $\tilde{\chi}_1^0$.

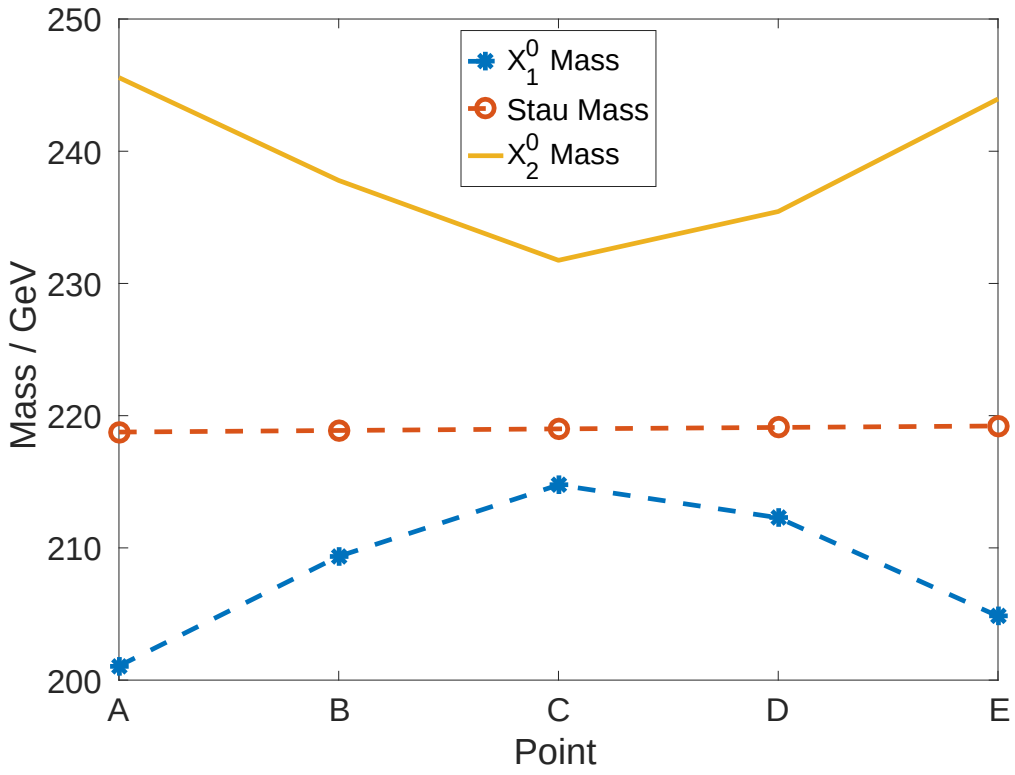

Figure 4: Plot showing mass variation across each N_{11} point. We can see that the mass hierarchy is consistent, which is important for this model, but that neutralino masses vary as the mixing matrix changes. Kinematic phase space reduces from A $\rightarrow$ C and widens from C $\rightarrow$ E. This has a calculable effect on cross section.

By reading in the individual lctuples into ROOT, there were many options available for analysis of the fragment particles. However when looking at particle branching ratios as a whole, the SPheno output files were more useful. For each point in N_{11}, the associated SPheno output would list the branching ratios and decay products of each particle. Then it was a simple task of using regular expressions to print out the data for the different particles I was interested in, so that separate analysis on their branching ratios could be carried out. In doing so I found that charginos provided a good route for measurement of the neutralino mixing matrix via branching ratio analysis. The branching ratio plot is shown as Figure 5.

From this plot we see that for low N_{11} values there is more variation in the decay products of the charginos, which provides us with an easier way to measure and differentiate between different points in the N_{11} space. For example if we measure that $\Gamma(\tilde{\chi}_1^{\pm} \rightarrow q\bar{q}) \approx 0.6\,\Gamma(\tilde{\chi}_1^{\pm})$, and $\Gamma(\tilde{\chi}_1^{\pm} \rightarrow e^{\pm}...) + \Gamma(\tilde{\chi}_1^{\pm} \rightarrow \mu^{\pm}...) \approx 0.4\,\Gamma(\tilde{\chi}_1^{\pm})$ then we can infer that we are around $N_{11} = 0.2$. However if we measure that $\Gamma(\tilde{\chi}_1^{\pm} \rightarrow q\bar{q}) \approx 0.65\,\Gamma(\tilde{\chi}_1^{\pm})$,

$\Gamma(\tilde{\chi}_1^\pm \to e^\pm ...) + \Gamma(\tilde{\chi}_1^\pm \to \mu^\pm ...) \approx 0.3\,\Gamma(\tilde{\chi}_1^\pm)$, and $\Gamma(\tilde{\chi}_1^\pm \to \tau^\pm ...) \approx 0.05\,\Gamma(\tilde{\chi}_1^\pm)$ then we can tell that we must be near to $N_{11} = 0.4$. We cannot do this for points above $N_{11} \approx 0.75$, because then the decay of the charginos becomes almost exclusively to $\tilde{\tau}$, meaning there is a drop off in the resolution with which we could tell the difference between different N_{11} values. But in this case this plot is also useful, because it tells us that if we measure $\Gamma(\tilde{\chi}_1^\pm \to \tilde{\tau} ...) \approx 1\,\Gamma(\tilde{\chi}_1^\pm)$, then we can essentially exclude values of N_{11} which are less than ~ 0.75 because they do not yield this branching ratio value.

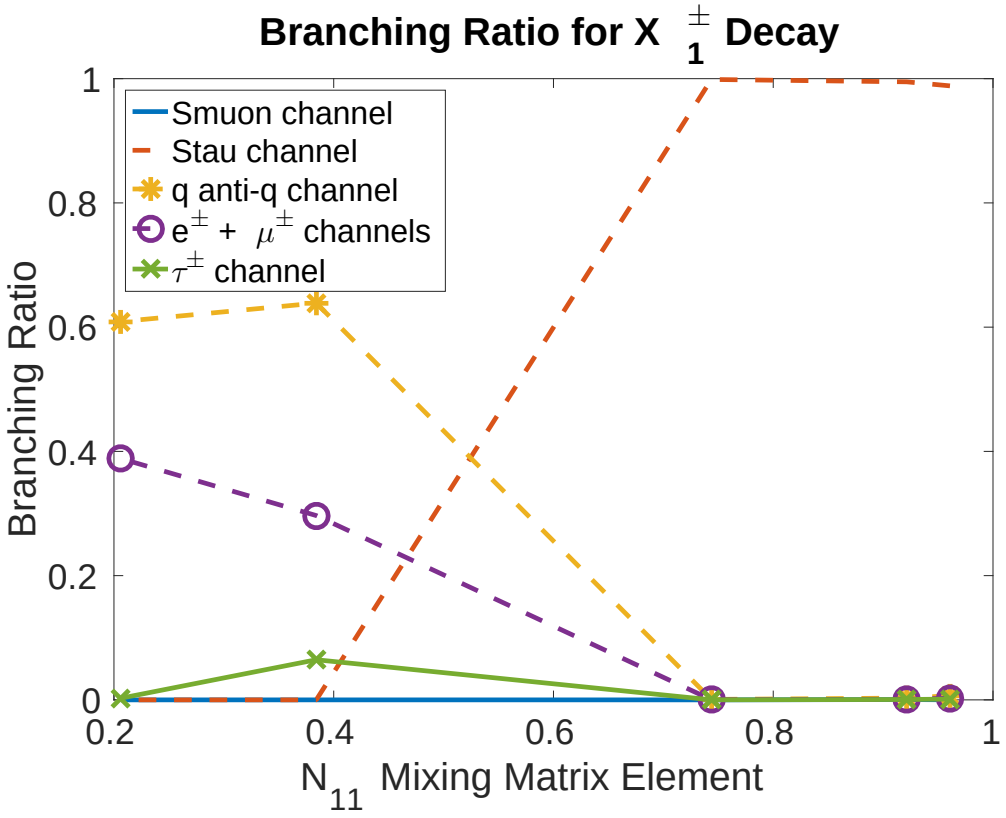

Figure 5: Plot showing chargino decay branching ratio across each N_{11} point. Optimal differentiation between different N_{11} values is for values below ~ 0.75. However it would be clear to rule out $N_{11} \lesssim 0.75$ if chargino decay was measured to be essentially exclusively to $\tilde{\tau}$.

3.4. Forward-backward asymmetry in chargino decay products

After looking primarily at the SPheno output files for the previous analysis, I now read in the associated LCTuples into ROOT for further analysis. Despite performing multiple sets of analysis on this data, and pursuing several different routes, only one unique method of neutralino mixing measurement was discovered. This involved measuring a kind of charge asymmetry in the chargino decay products. By checking the generator

status of the particle in each event (1 indicates final state particle, whereas 2 indicates that it will fragment further) I could ensure that I looked only at final decay products. I simultaneously applied a check that only let through the charged leptons, $e^{\pm}, \mu^{\pm}, \tau^{\pm}$ by using the PDG number variable in the LCTuple. If these checks were passed then the angular direction was calculated from the momentum components of the particle, and this quantity was multiplied by the charge of the lepton in question. This quantity was indeed found to vary depending on which point in the N_{11} space we were considering, making it a viable option for the direct experimental measurement of the neutralino mixing.

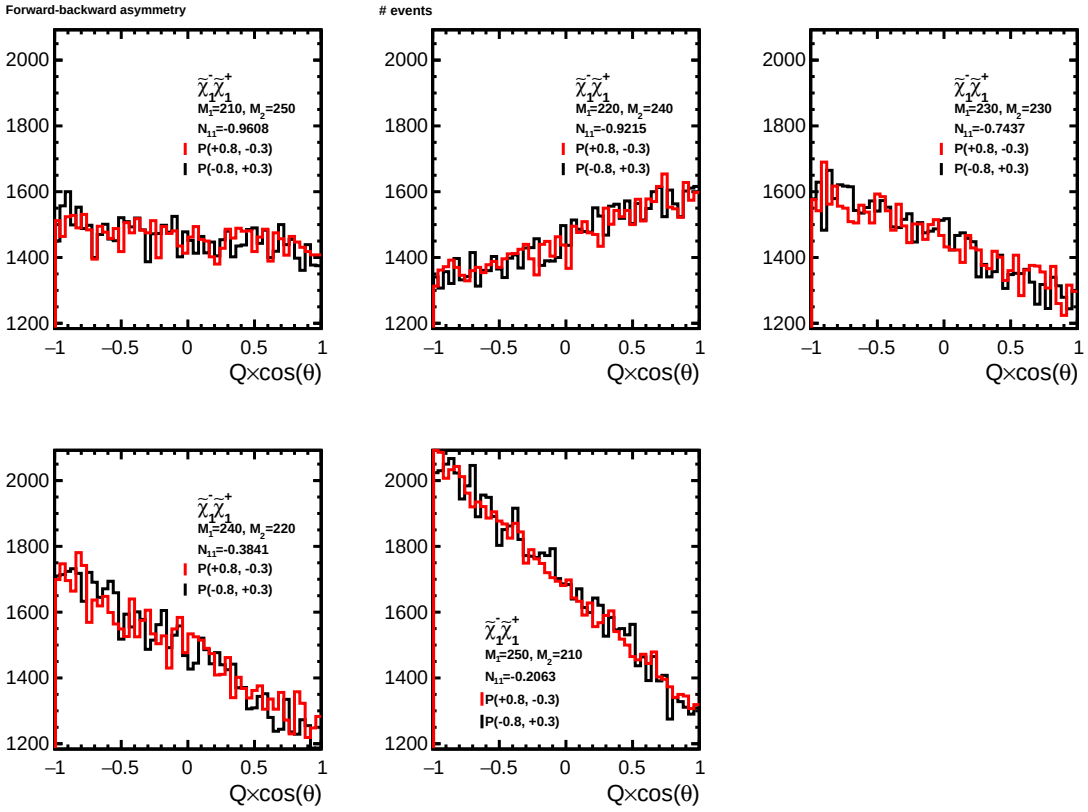

Figure 6: Plot showing chargino decay product charge/directional asymmetry versus N_{11} point. The plots are presented for the points in the order A $\rightarrow$ E being read right to left and up to down. Axes labels read number of events on the y axis, and $Q \times \cos(\theta)$ on the x axis. The red line indicates the $\mathcal{P}(+0.8, -0.3)$ polarised beam combination, and the black line represents $\mathcal{P}(-0.8, +0.3)$. The other data presented on each graph's legend is the M_1 and M_2 point and the value of N_{11}.

At large N_{11} the distribution is fairly flat, with no indication of a preferred direction or charge. However this soon changes at N_{11} begins to decrease, and there is a pre-

ferred charge × direction combination in the forward direction. Between point B and C this preferred peaking switches to the negative combination of charge and angular direction. As N_{11} continues to fall from point C this trend continues, with the preferred charge-direction product peaking more and more negatively. By measuring this quantity's distribution we could potentially determine N_{11}. For example if we measure the distribution to be flat, we may know that we are near to $N_{11} \approx -1$. However, as we see a switchover in direction between points B and C, there must be at least one more horizontal region, so this will need to be considered more carefully if this method is to be used to measure the neutralino mixing. For example, running similar calculations for more than five points may be able to show us how limited we are in distinctly identifiable N_{11} points for this observable's method. Furthermore, this method's predictions do not change based on the beam polarisation, unlike the first method. This means that we cannot add the extra layer of experimental validation that can be gained by switching the beam polarisation and remeasuring the distribution to see if the other prediction is also met.

4. Conclusion & Outlook

4.1. Conclusion

This project aimed to identify methods of direct experimental measurements of the neutralino mixing matrix elements, especially N_{11}. The motivation for this is because it was found that the dark matter relic density is particularly senstitive to this parameter [2]. The hope is that measuring N_{11} will allow us to tie down the value of the dark matter relic density accounted for by the LSP, and in doing so either prove or disprove that it is the sole contributor to the measured relic density.

To this end the MSSM parameter space was scanned near the previously studied STC8 point, to find points where the neutralino mixing matrix varied. For each of these points the Whizard event generator created 100 000 events for four different channels with two polarisations each. These data sets were then analysed to see which experimental observables indicated best the change in neutralino mixing.

Three such experimental observables were identified as being particularly useful in probing the neutralino mixing. The first method was the cross section of production processes, with $e^+e^- \to \tilde{\chi}_1^0\tilde{\chi}_2^0$ being focused on in this report. The second was the branching ratio of particles produced in the e^+e^- collision, with the decay of charginos being focused on in this report. Finally, the forward-backward asymmetry of the leptonic decay products of generated charginos was examined.

Each of these processes came with caveats which make them more or less useful in different scenarios. If the ILC discovers a similar version of SUSY as that discussed in this study, then all of these methods provide useful methods of probing neutralino mixing properties, and could potentially be used to verify each other.

4.2. Outlook

This study was relatively qualitative in nature. In the future a more quantitative study could be done, with an increase in the number of points from which events were generated. This would give finer resolutions between the different N_{11} points. Presumably there will come a point where one is no longer able to tell the difference between the experimental observables at different N_{11} values, as the graphical changes will be too subtle. Thus one will lose the ability to differentiate between these two values by measuring the experimental observables. Determining this resolving power of sorts will in turn determine the limit of the accuracy of measurement of N_{11} using these methods. If this accuracy is too limiting, then it may not be possible to match the accuracy of the ESA Planck mission's determination of the relic density, and hence this experimental option will not be able to confirm or deny that the LSP is the only contributor to dark matter.

Appendix A Numerical results

Point	A	B	C	D	E
M1	210	220	230	240	250
M2	250	240	230	220	210
N_{11}	-0.9608	-0.9215	-0.7437	-0.3841	-0.2063
N_{12}	0.1662	0.2868	0.5801	0.8541	0.9219
N_{21}	-0.2305	-0.3534	0.6467	0.9059	0.9602
N_{22}	-0.9230	-0.8988	0.7502	0.4220	0.2552
$\tilde{\chi}_1^0$ mass	201.07	209.36	214.76	212.28	204.84
$\tilde{\tau}_1^-$ mass	218.76	218.88	219.00	219.11	219.22
$\tilde{\chi}_2^0$ mass	245.57	237.79	232.75	235.44	243.95
$\tilde{e}_L^-$ mass	310.71	310.50	310.30	310.10	309.92
$\tilde{e}_R^-$ mass	227.11	227.24	227.38	227.51	227.64
$\tilde{\mu}_L^-$ mass	310.71	310.50	310.30	310.11	309.93
$\tilde{\mu}_R^-$ mass	227.10	227.24	227.37	227.50	227.63
$\tilde{\tau}_2^-$ mass	312.97	312.77	312.59	312.41	312.25
$\tilde{\chi}_2^0 \to (\tilde{e}_R^\pm, \tilde{\mu}_R^\pm)(e^\mp, \mu^\mp)$ BR	0.3464	0.3387	0.2466	0.2060	0.4744
$\tilde{\chi}_2^0 \to \tilde{\tau}_1^\pm \tau^\mp$ BR	0.6535	0.6613	0.7534	0.7940	0.5252
$\tilde{\chi}_1^\pm \to \tilde{\mu}_R^+ \nu_\mu$ BR	0.0001	0.0005	0	0	0
$\tilde{\chi}_1^\pm \to \tilde{\tau}_1^+ \nu_\tau$ BR	0.9884	0.9949	0.9987	0	0
$\tilde{\chi}_1^\pm \to \tilde{\chi}_1^0 q\bar{q}$ BR	0.0067	0.0029	0.0008	0.6387	0.6090
$\tilde{\chi}_1^\pm \to \tilde{\chi}_1^0 (e^+, \mu^+)(\nu_e, \nu_\mu)$ BR	0.0026	0.0011	0.0003	0.2967	0.3884
$\tilde{\chi}_1^\pm \to \tilde{\chi}_1^0 \tau^+ \nu_\tau$ BR	0.0013	0.0006	0.0001	0.0646	0.0027

Appendix B Generalisation to other N_{ij} elements

The method of generating plots which show graphical differences in the N_{11} value in order to see which experimental variables depend on its value can also be considered for other matrix elements. In this example the cross section for $\tilde{\chi}_1^0\tilde{\chi}_2^0$ production versus the matrix elements (clockwise) N_{11}, N_{12}, N_{21} and N_{22}. This generalised treatment was carried out throughout the whole analysis, but was simplified to just N_{11} in this report for the sake of presentation, brevity and clarity, and also because of the particular importance of the N_{11} value in determining the relic density.

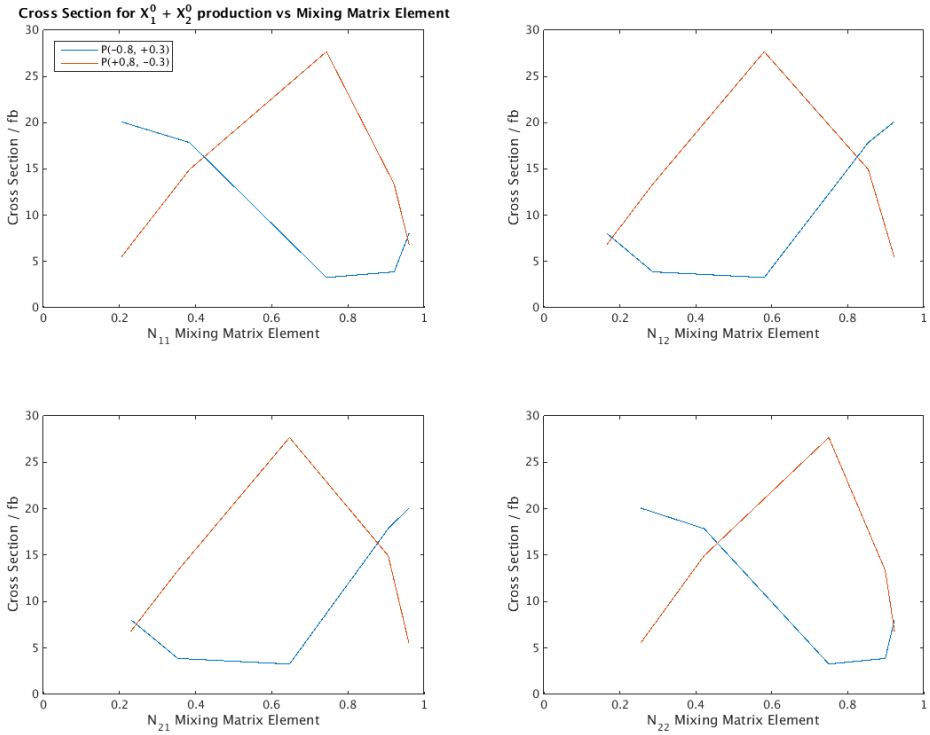

Figure 7: An example of one of the plots generated considering more matrix elements than just N_{11}. All of the other results could be generalised in such a way, leading to the direct experimental measurement of other neutralino mixing matrix elements.

References

[1] Ade, P. A. R.; Aghanim, N.; Armitage-Caplan, C.; (Planck Collaboration); et al. (22 March 2013). "Planck 2013 results. I. Overview of products and scientific results Table 9". Astronomy and Astrophysics. 1303: 5062. arXiv:1303.5062. Bibcode:2014A&A...571A...1P. doi:10.1051/0004-6361/201321529.

[2] Suvi-Leena Lehtinen, Mikael Berggren, Jenny List. "Dark matter relic density from observations of supersymmetry at the ILC". International Workshop on Future Linear Colliders (LCWS15). arXiv:1602.08439

[3] "The International Linear Collider Gateway to the Quantum Universe" (PDF). ILC Community. 2007-10-18

[4] B. Aurand et al. "Beam Polarization at the ILC: the Physics Impact and the Accelerator Solutions" DESY 09-042 arXiv:0903.2959

[5] Werner Porod "SPheno, a program for calculating supersymmetric spectra, SUSY particle decays and SUSY particle production at e+ e- colliders" Comput.Phys.Commun.153:275-315,2003 arXiv:hep-ph/0301101

[6] J. Reuter et al. "Modern Particle Physics Event Generation with WHIZARD" Proceedings of the conference "ACAT 2014 (Advanced Computing and Analysis Techniques in physics)" arXiv:1410.4505

[7] Torbjrn Sjstrand et al. "An Introduction to PYTHIA 8.2" 11 Oct 2014 FERMILAB-PUB-14-316-CD arXiv:1410.3012

[8] Martin, Stephen P. (1997). "A Supersymmetry Primer". arXiv:hep-ph/9709356.

[9] David, Curtin (August 2011). "Model Building and Collider Physics Above the Weak Scale" Cornell University.

[10] Martin, Stephen P. "Extra vector-like matter and the lightest Higgs scalar boson mass in low-energy supersymmetry" Phys.Rev. D81 (2010) 035004 arXiv:0910.2732 [hep-ph] FERMILAB-PUB-09-852-T

[11] M. E. Peskin "Will there be supersymmetry at the ILC?" July 2012, LHC Implications, CERN

[12] Jonathan L. Feng, Mihoko M. Nojiri. "Supersymmetry and the Linear Collider". A chapter in Linear Collider Physics in the New Millennium, published by World Scientific. arXiv:hep-ph/0210390

[13] G. Jungman, M. Kamionkowski, K. Griest. "Supersymmetric Dark Matter" Phys.Rept. 267 (1996) 195-373 arXiv:hep-ph/9506380 DOI:10.1016/0370-1573(95)00058-5

[14] G. Belanger, F. Boudjema, A. Pukhov, A. Semenov. " micrOMEGAs: A program for calculating the relic density in the MSSM" Comput.Phys.Commun. 149 (2002) 103-120 DOI: 10.1016/S0010-4655(02)00596-9 arXiv:hep-ph/0112278